Promoting sensitivity and selectivity of HCHO sensor based on strained InP_3 monolayer A DFT study

Yang, Huiru; Wang, Zeping; Ye, Huaiyu; Zhang, Kai; Chen, Xianping; Zhang, Guoqi

DOI
10.1016/j.apsusc.2018.08.014

Publication date
2018

Document Version
Accepted author manuscript

Published in
Applied Surface Science

Promoting sensitivity and selectivity of HCHO sensor based on strained InP_3 monolayer: A DFT study

Huiru Yang,[1] Zeping Wang,[1] and Huaiyu Ye,*[1,2] Kai Zhang,*[3] Xianping Chen,[1, 2] Guoqi Zhang[2]

[1]Key Laboratory of Optoelectronic Technology & Systems, Education Ministry of China, College of Opto-electronic Engineering, Chongqing University, Chongqing 400044, China.

[2]Electronic Components, Technology and Materials, Delft University of Technology, 2628 CD Delft, The Netherlands.

[3]School of Electro-mechanical Engineering, Guangdong University of Technology, No.100 Waihuan Xi Road, Guangzhou Higher Education Mega Center, Guangzhou, 510006, China.

*Corresponding authors: huaiyuye@tudelft.nl; zhangkai@gdut.edu.cn.

Abstract

Sensitive materials for formaldehyde (HCHO) sensor need high sensitivity and selectivity. The research on two dimensinal (2D) sensitive material is growing, and most studies focus on the pristine or modified graphene. So it is essential to introduce other 2D materials into HCHO gas sensor. In this report, the adsorption behaviors of organic gas molecules including C_2H_6, C_2H_4, C_2H_2, C_6H_6, C_2H_5OH and HCHO over indium triphosphide (InP_3) monolayer were studied by using first-principle atomistic simulations. The calculation results demonstrate that InP_3 monolayer has a high sensitivity and selectivity to HCHO than others. By comparing the structures and adsorption results of InP_3 monolayer, graphene and single-layered MoS_2, it was found that the polarity bonds and steric effect of the site on monolayer play an important role in the detection of HCHO. The effect of strain on the gas/substrate adsorption systems was also studied, implying that the stained InP_3 monolayer could enhance the sensitivity and selectivity to HCHO. This study provides useful insights into the gas-surface interaction that may assist future experimental development of 2D material for HCHO sensing and performance optimization based on strain.

Keywords: First-principles calculation; HCHO sensing; InP_3 monolayer; strain

1 Introduction

Formaldehyde (HCHO) is one of the most harmful volatile organic compounds (VOCs), and is usually discharged from many products that are widely used in the world [1]. Long exposure to the air containing a certain amount of HCHO may cause harmful impacts on human health. To quickly and accurately detect HCHO, both sensitive material and sensing mechanism are necessary to be developed and a lot of efforts had been made in this research field [2-4]. From the point of view of sensitive material, a series of metal oxide semiconductors have been reported, such as TiO_2, ZnO, SnO_2, In_2O_3 and so on [3, 5, 6]. The investigations on innovative chemical materials have also brought metal-organic frameworks [7] and carbon nanotube [8] into such a research field. Although these materials have the ability of HCHO detecting, they still have some limitations such as low relative resistance changes, low selectivity and long-term instability and so on. Thus, the study on the sensitive materials to HCHO will never stop.

The discovery of graphene has shed a new light on the investigation of the sensitive material for HCHO detecting, for its ultra-thin structure, huge specific surface area, high conductivity and low electrical noise [9-11]. The two-dimensional (2D) materials with large surface area are believed can be fully in contact with the gas, and more conducive to enhance the performance of the gas sensor. Regrettably, the interaction between graphene and HCHO was found to be pretty weak [12, 13], which may limit the further enhancement

of the graphene-based sensor performance. To solve this problem, some efforts have been made by compositing graphene with metal oxide or metal nanoparticles [13, 14]. However, it seems that the related research is limited in pristine or modified graphene. The family of 2D material is growing rapidly in recent years, including silicone [15], germanane [16], phosphorus allotropes [17, 18], MXenes, and transition-metal dichalcogenides (TMDs) [19, 20]. Therefore, extending the research to other 2D materials is a promising way and may help us find a more sensitive material for HCHO detecting.

The recently predicted InP_3 monolayer [21] is a new category of layered indirect-band gap semiconductor, which has been theoretically discovered by Miao *et al.* and expected to be fabricated experimentally from its layered bulk crystal by exfoliation for the moderate exfoliation energy. The synthesis and crystal structure of bulk InP_3 was first reported by Kinomura, and the bulk InP_3 is stability at ambient conditions [22]. With a suitable band gap (1.14 eV), high electron mobility (1919 $cm^2 \cdot V^{-1} \cdot s^{-1}$), high-mobility transport anisotropy (armchair and zigzag direction) and great optical performance, it suggests that the 2D InP_3 is a promising candidate material for future applications in electronics and optoelectronics [21]. Recently, Liu and co-workers [23] theoretically predicted monolayer InP_3 as a reversible anode material for ultrafast charging lithium- and sodium-ion batteries.

From the perspective of the sensing mechanism, the semiconductor type gas sensor works based on the change of the conductivity of the sensitive material

caused by adsorption of gas molecules onto its surface [3, 24]. In order to increase the detection limit of this type gas sensor, an effective method is to enhance the interaction between gas molecules and sensitive materials, and the resulting stronger adsorption and more charge transfer will lead to greater changes in conductivity, which in turn will increase sensitivity [25]. It was also found that the gas-sorbent interaction and gas-sensing characteristic depend largely on the surface structure and properties of the sensitive materials. The structure of InP_3 is closely related to that of arsenic, replacing systematically every fourth atom in the arsenic layer by an indium (In) atom and the rest by phosphorus (P) atom. Their monolayer structures are similar, except that the surface of arsenene [26] is composed only of As atoms, while the compositions of InP_3 monolayer are P and In atoms. To the best of our knowledge, surface component of most 2D materials is single element. Take TMDs and MXenes as examples, their monolayers are composed of separate metal and non-metal atomic layers. While in InP_3, every layer is consisted of both metal atoms (In) and non-metal atoms (P). It can be speculated that the unique structure of InP_3 monolayer may cause rather different gas sensing behaviour. Therefore, it is of necessity to theoretically study the interaction between the surface of this sensitive material and gas molecules. In this regard, calculation based on the first principle can provide reliable information such as adsorption energy and electronic properties of the adsorption system. In addition, the calculation of adsorption of NO_x on ZnO [6, 27], and SO_2 on graphene have been completed, which make sure theoretical calculation is a powerful tool that

can help us to choose the sensitive material and experiment routine. Meanwhile, the modification of surface structure by doping and strain has been proposed and demonstrated as an efficient way to modify the electronic, magnetic, chemical, and sensing properties of materials [28, 29].

In this work, the adsorptions of HCHO and its various possible organic interfering gases (including C_2H_6, C_2H_4, C_2H_2, C_6H_6 and C_2H_5OH) on InP_3 monolayer were calculated based on density functional theory (DFT) simulations. To explore the sensitivity and selectivity of gas sensor based on InP_3, The properties of the gas/InP_3 adsorption systems including adsorption energy (E_a), adsorption distance (d), charge transfer (ΔQ), total and partial densities of states (DOS and PDOS) and recovery time were calculated. The possible sensing mechanism was also explored by comparing the adsorption of HCHO on three types of 2D materials (graphene, single-layered MoS_2 and InP_3 monolayer) with different structure features. The study on the adsorption site of HCHO and the steric effect of the site on sensitive materials were condected, indicating that structure of sensing material plays an important role in the detection of HCHO. Then, the performance optimization of HCHO sensor was also performed by applying strain on InP_3 monolayer, which shows that strained InP_3 monolayer is more sensitive and selective to HCHO.

2 Computational details

The first-principle calculations of structural optimization and electronic properties are performed on the basis of DFT as implemented in the DMol^3

package. The exchange correlation interaction is treated through a general gradient approximation (GGA) with the Perdew−Burke−Ernzerhof (PBE) function [30]. The dispersion corrected DFT-D proposed by Grimme has been employed in order to investigate the interactions between the organic gas molecules and monolayer material. The convergence criteria of self-consistent field energy, the MAX force and the maximum displacement are 1.0×10^{-5} eV, 0.002 eV/Å, and 5.0×10^{-3} Å, respectively. The Brillouin zone integration is done by setting a $12\times12\times1$ Monkhorst-Pack *k*-point grid for a $2\times2\times1$ InP_3 supercell for both geometry optimization and electronic properties calculations, while the structure of graphene is obtained on the foundation of a $4\times4\times1$ supercell. The thickness of a vacuum region in the Z direction is kept as 20 Å to avoid the effect of interaction deriving from the adjacent layer.

The adsorption energy (E_a) is defined as follows:

$$E_a = E(\text{sub+gas}) - E(\text{sub}) - E(\text{gas}) \qquad (1)$$

where E(sub+gas), E(sub) and E(gas) are the total energy of gas/substrate adsorption system, isolated substrate and the separated organic gas molecules, respectively.

The adsorption distance (d) is defined as the vertical distance between the lowest atom of the gas molecule and the top atom of InP_3 monolayer. The charge transfer (ΔQ) of the gas molecules adsorbed on InP_3 monolayer can be studied using Mulliken population analysis [31]. A positive value of ΔQ means the charges transfer from gas to the surface of substrate.

The charge density difference (CDD) is calculated by the following formula:

$$\Delta\rho = \rho(\text{sub+gas}) - \rho(\text{sub}) - \rho(\text{gas}) \quad (2)$$

where ρ(sub+gas), ρ(sub) and ρ(gas) are the charge densities of the gases adsorption system, substrate, and separated organic gas molecule, respectively.

The electron localization function (ELF) is carried out using CASTEP code. The energy cutoff is set as 500.0 eV and the ultrasoft pseudopotentials are adopted.

3 Results and discussion

We first tested the accuracy of our computational method by calculating the lattice constants of unit cell of InP_3 monolayer and graphene. The values are 7.535 Å and 2.466 Å, respectively, which are in agreement with the previously reported results [21, 32, 33].

3.1 The adsorption of organic gases on InP_3 monolayer

To explore possible sensitivity and selectivity of InP_3 monolayer to HCHO, C_2H_6, C_2H_4, C_2H_2, C_6H_6, C_2H_5OH and HCHO are chosen as adsorbates. The adsorption sites and configurations are determined by analysing the structure feature of InP_3 monolayer.

InP_3 monolayer exist two kinds of six-membered rings, one is formed by six P atoms (R1) and the other includes four P atoms and two para-position In atoms (R2). As shown in Fig. 1(a), each In atom is bonded with three P atoms from three separate R1s and each P atom is bonded with one In atom. There are also two kinds of In and P atoms due to both two rings are exhibit chair

conformation, which are named as In1, In2, P1 and P2, respectively. Considering the complexity of InP_3 monolayer structure, a number of adsorption sites including P1 atom, P2 atom, In1 atom, In2 atom, the centre of R1 and the centre of R2 are taken into account with a reason that gas molecules with different structures tend to be adsorbed in different sites and configurations. To this end, the single gas molecule of C_2H_6, C_2H_4, C_2H_2, C_6H_6, C_2H_5OH and HCHO was placed at a distance of 3Å above the adsorption sites mentioned above to find the one with lowest adsorption energy. At these particular positions, several molecular orientations were also considered. Take HCHO molecule as an example, three orientations of the HCHO molecule were investigated, with the H atom, O atom and C atom pointing to the surface of InP_3, respectively.

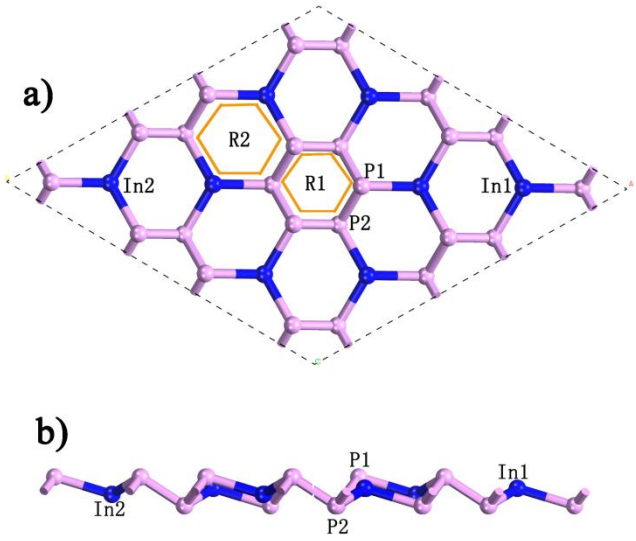

Fig. 1 Top (a) and side (b) view of the optimized structural (supercell) model of InP_3 monolayer

The interaction between gas and InP_3 monolayer can be described regarding their E_a. Based on Eq. (1), the more negative the value of E_a is, the stronger

adsorption of gas molecules on InP_3 would be. The most energetically favourable adsorption configurations for all gases mentioned above are selected for further studies, and Fig. S1 presents the lowest energy configurations. And the E_a aforementioned of gas molecules onto InP_3 monolayer, the adsorption distances, and the charge transfers are listed in Table 1.

Table 1 Adsorption energy (E_a), adsorption distance (d), charge transfer (ΔQ) and the related covalent radii (r) between InP_3 monolayer and organic gas molecules (C_2H_6, C_2H_2, C_2H_4, C_6H_6, C_2H_5OH, and HCHO)

Gas molecule	E_a(eV)	ΔQ (e)	d(Å)	r(Å)
C_2H_6	-0.3118	-0.07	2.819	2.44(H-In)
C_2H_4	-0.7488	0.063	2.672	2.52(C-In)
C_2H_2	-0.5867	0.088	2.718	2.52(C-In)
C_6H_6	-0.9290	0.004	2.752	2.52(C-In)
C_2H_5OH	-1.1186	0.175	2.322	2.32(O-In)
HCHO	-1.2974	-0.368	1.933	2.12(C-P)

For C_2H_6 molecule, the steadiest configuration is presented in Fig. S1(a), where the C-C single band seemingly parallel to the monolayer and the adsorption distance is 2.819 Å. In the case of C_2H_4 adsorption, the most favourable adsorption configuration based on the lowest adsorption energy is exhibited in Fig. S1(b), where the plane of C_2H_4 molecule is aligned parallel to InP_3 monolayer surface with the C-C double band directly above the In1 atom. The configuration of C_2H_2 adsorption is similar to C_2H_4, Fig. S1(c) shows the C-C triple band directly above the In1 atom and the adsorption distance is 2.718 Å, larger than that of C_2H_4 (2.672 Å). All atoms of C_6H_6 are in a plane that is not parallel to InP_3 monolayer and forms a specific angle, as shown in Fig.

S1(d). Fig. S1(e) shows the adsorption configuration of C_2H_5OH molecule, where O atom closes to In1 atom. These adsorption systems hardly caused deformation of the InP_3 monolayer. While for HCHO, the structures of both HCHO molecular and monolayer have changed. HCHO prefer to locate parallel to the monolayer with O atom upon In1 atom and C atom upon P1 atom, and the distance between In1 and P1 ($d1$ = 3.392 Å) is smaller than others (from $d2$ to $d6$), as shown in Fig. S1(f).

According to the calculation results, adsorption strength changes in the following order: HCHO > C_2H_5OH > C_6H_6 > C_2H_4 > C_2H_2 > C_2H_6. The E_a (-1.2974 eV) of HCHO is the most negative one, implying that InP_3 monolayer exhibits excellent HCHO gas sensing performance. Besides, the charge transfer of HCHO (-0.368 e) is the largest of all studied gases. This means that when HCHO adsorbed on InP_3 monolayer, it may cause large changes in the electrical signal, resulting in a lower detection limitation. The HCHO molecule behaves as electron acceptors for the charges transfer from the substrate to it.

For C_2H_5OH/InP_3 adsorption system, the absolute value of E_a (1.1186 eV) and ΔQ (0.175 e) are obtained, which are smaller than that of $HCHO/InP_3$ system, but are still larger than the values of other four hydrocarbons gases. The distances are 1.933 Å and 2.322 Å for $HCHO/InP_3$ and C_2H_5OH/InP_3, respectively. They are less than the sum of covalent radii (2.12 Å for In-O and 2.32 Å for In-C), indicating that HCHO may be chemisorbed on InP_3 monolayer. The difference between HCHO and C_2H_5OH when adsorbed on

InP_3 monolayer may be due to the steric effect of the hydrogen atoms on the hydroxyl groups in C_2H_5OH, preventing C_2H_5OH and InP_3 monolayer from getting closer. Therefore, the interaction between HCHO and the substrate is stronger than C_2H_5OH.

Compared with these two oxygen-containing molecules, the absolute value of E_a and ΔQ of other four hydrocarbons molecules are much lower. For C_6H_6/InP_3 adsorption system, the E_a is -0.9290 with a ΔQ of 0.004 e, which suggests that C_6H_6 adsorption strength is weak. When C_2H_4 adsorbed on InP_3 monolayer, there is a relatively large adsorption strength (-0.7488 eV) and charge transfer (0.063 e) among hydrocarbon molecules. And the adsorption distance is 2.672 Å, which is greater than the sum of their covalent radii (2.52 Å). This may means that all these hydrocarbon molecules are physically adsorbed on InP_3 monolayer.

In this part we focus primarily on exploring the deeper interaction mechanism between adsorbates and InP_3 monolayer. The charge density difference (CDD) of C_2H_4/InP_3, C_2H_5OH/InP_3 and $HCHO/InP_3$ adsorption systems were calculated and presented in Fig. 2(a)(b)(c), the charge accumulation is represented by green colour, whereas yellow represents the charge depletion region. As shown in Fig. 2(a), there is rarely charge density redistribution between C_2H_4 and InP_3 monolayer, implying that their interaction is weak and no chemical bond is formed. While for oxygen-containing gases, the charge density redistribution is more obvious, and the most apparent is HCHO

adsorption. Fig. 2(b) shows that the charge density redistribution of C_2H_5OH/InP_3 adsorption system. In Fig. 2(c), the charge density redistributes of the $HCHO/InP_3$ system is mainly induced by the strong interaction between O atom of HCHO molecule and In1 atom of InP_3 monolayer. There is a significant depletion of charge density between O atom and In atom, suggesting the covalent bond may partly formed between HCHO and InP_3 monolayer.

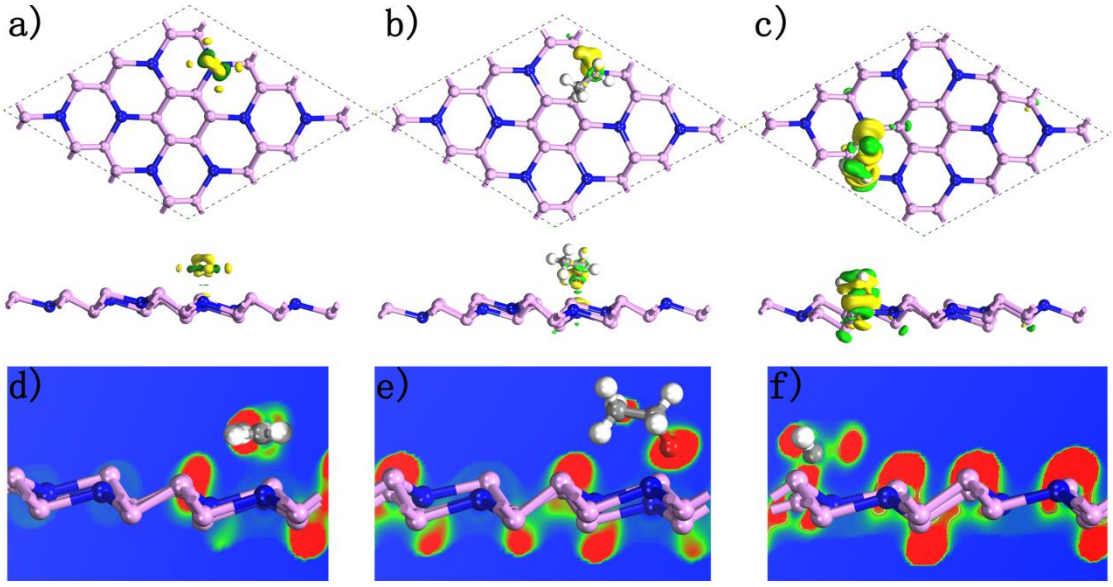

Fig.2 The CDD of (a) C_2H_4, (b) C_2H_5OH and (c) HCHO on InP_3 monolayer. The isosurface value is 0.02 e/Å^3. The green region shows the charge accumulation, whereas the yellow region represents the charge depletion. (d)(e)(f) present the corresponding ELF plots.

Besides, the corresponding ELF charts of the above three systems are presented in Fig. 2(d)(e)(f). As shown in Fig. 2(d), the electron localization of InP_3 monolayer and C_2H_4 is separated, further demonstrating that there is no chemical bond between C_2H_4 gas and the monolayer. The interaction between C_2H_4 and InP_3 is composed by weak van der Waals force, and it is quite sure that C_2H_4 is physical adsorbed on InP_3. As shown in Fig. 2(e), the ELF of C_2H_5OH/InP_3 system is similar to C_2H_4/InP_3 system, and the electron localization does not overlap, which means that there may also no chemical

bond formed between C_2H_5OH and InP_3 monolayer. While for HCHO, the overlap of electron localization means that adsorption of HCHO is stronger than other gases and may chemisorption, further illustrating that the material is more sensitive to HCHO, Fig. 2(f).

To further explore the sensitivity of InP_3 monolayer towards HCHO gas molecule, DOS, PDOS and band structure were calculated and described in Fig. 3. After adsorption of HCHO on InP_3, significant change of DOS near Fermi level can be seen from Fig. 3(a). The adsorption of HCHO leads to noticeable perturbation to the DOS of InP_3 substrate, including the movement of peaks and the generation of new peaks. Simultaneously, there are orbital hybridizations according to the states of O-2p, P-3p and In-5p orbitals between −2 and 0 eV; and other two orbital hybridizations between 0 and 3.5 eV, not only including C-2p, P-3p, In-5s and In-5p but also O-2p, P-3s, P-3p and In-5p. These make clear that the sensitivity of InP_3 to HCHO. From the changes of band structure, Fig. 3(b), it is noted that the adsorption of HCHO onto InP_3 causes the conduction bands to move slightly towards higher energy level, indicating that the band gap of HCHO/InP_3 system slightly increased from 0.741 eV to 0.780 eV and the conductivity has a slight decrease compare with that of isolated InP_3.

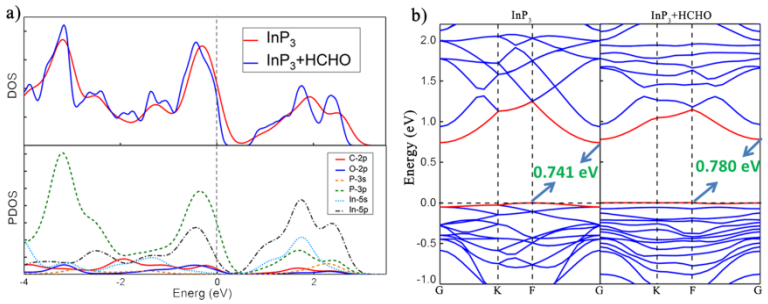

Fig. 3.(a) DOS (up) of InP_3 with and without HCHO, and PDOS (down) of HCHO/InP_3 system. (b) Band structures of pristine InP_3 (lift) and HCHO adsorbed on pristine InP_3 (right).

The analysis of E_a, d, ΔQ, CDD and ELF indicate that the adsorptions of oxygen-containing gases onto InP_3 monolayer are much more effective than that of oxygen-free gases, which is consistent with the previous reported experiment results [5, 25, 34, 35], that is, the sensitive materials of HCHO sensor are sensitive to oxygen-containing gases than oxygen-free gases. Then the deeper understanding of the interaction mechanism between adsorbates and InP_3 monolayer is essential, which will helpful in further enhancing the performance of HCHO sensor.

3.2 Adsorption of HCHO on different 2D materials

In this section, the other two 2D materials with different structures, namely graphene and single-layered MoS_2, were selected as the substrate for adsorbing HCHO. The adsorptions of a single HCHO molecular on the top of these layer materials were compared with each other and the configurations with the largest absolute value of adsorption energy (E_a) were presented in Fig. 4, the values of E_a, d and ΔQ were also listed in Table 2. In order to find out the structural feature causing the strong interaction between HCHO and InP_3 monolayer, an

in-depth comparison and analysis of the structural differences and corresponding calculation results of these three materials was conducted.

Table 2 Adsorption energy (*E*a), adsorption distance (*d*), and charge transfer (Δ*Q*) between HCHO and 2D materials (InP_3 monolayer, graphene and single-layered MoS_2).

substance	E_a (eV)	*d* (Å)	Δ*Q* (e)
InP_3	-1.2974	1.933	-0.368
graphene	-0.0716	2.993	0.016
MoS_2	-0.03	3.74	0.01

In Fig. 4(a), HCHO molecule is perpendicular to the surface of graphene. Fig. 4(b) shows HCHO/MoS_2 system, the HCHO molecular is seemingly parallel to the surface of MoS_2 monolayer. In HCHO/InP_3 system, the HCHO is also seemingly parallel to the surface of InP_3 monolayer with O atom upon In1 atom and C atom upon P1 atom, as shown in Fig. 4(c). The structure of HCHO has also changed, that is, the four atoms of a simple HCHO molecule without adsorption are in the same plane, while HCHO of the adsorption system is not a planar molecule. The largest absolute value of E_a and Δ*Q* for HCHO on InP_3 are 1.2974 eV and -0.368 e, respectively, which are larger than the corresponding values of HCHO on graphene (0.0716 eV and 0.016 e) and MoS_2 (0.03 eV and 0.01 e) [36].

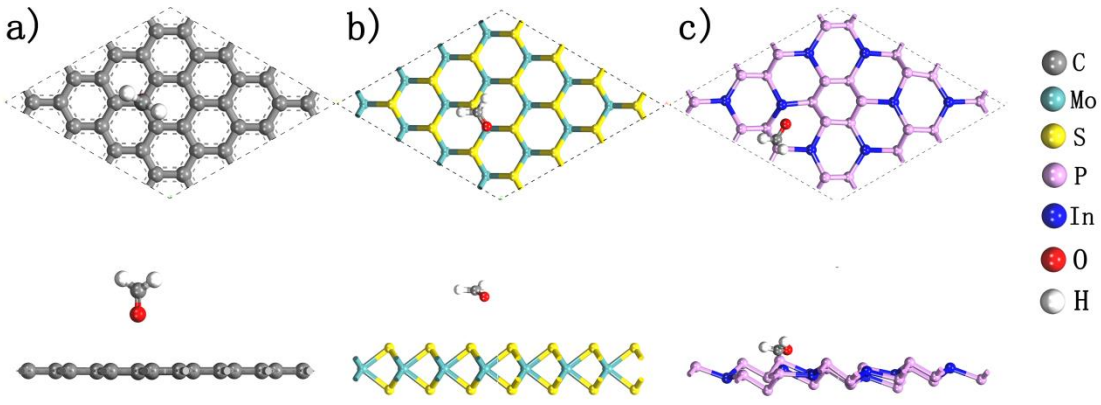

Fig. 4 The structure of HCHO adsorbed onto (a) graphene, (b) single-layered MoS_2 and (c) InP_3 monolayer.

3.2.1 The influence of electronegativity

The weak adsorption of HCHO onto graphene and single-layered MoS_2 may result from the large electronegativity of C (2.55) and S (2.58). As shown in previous reports, HCHO molecule often behaved as an electron acceptor and thus the strong interaction between HCHO and the substrates often involve significant electron transfer from the substrates to the molecule and the charge transfer is negative [12-14, 36]. As a result, the large electronegativity of S atom may make it difficult for HCHO to grab electrons from MoS_2 and thus prevent the strong interaction between them. The adsorption of HCHO onto graphene is similar. Compared with C and S atom, the electronegativity of In atom (1.78) is smaller, which may be a reason why adsorption of HCHO onto InP_3 monolayer is stronger than that of graphene and single-layered MoS_2.

3.2.2 The influence of structure and polar bond

On the other side, the difference of interaction between HCHO and these 2D materials is related to the difference in materials' structures, which can be seen from Fig. 4. Graphene is composed of a hexagonal-close-packed carbon network, in which each atom covalently bonds to three neighbouring ones

through σ-bond [37], and a theoretically plane with uniformly distributed charge is formed, Fig. 4(a). The monolayer structure of MoS_2 is shown in Fig. 4(b), and it is consist of three atomic layers, one Mo layer and two S layers [38, 39]. The Mo layer is electropositive and the S layers are electronegative, then the Mo layer is sandwiched between two S layers and seems like shielded by them. Besides, InP_3 monolayer is a puckered honeycomb structure, the surface of which is composed of In and P atoms, Fig. 4(c).

Since HCHO is a polar molecule and the O atom has a large electronegativity, when this molecule was placed on graphene that is a nonpolar substance, the interaction between them may be only dispersion force and induction force. These forces are both very weak. MoS_2 is also a non-polar molecule, however, its chemical bonds are polar and there are dipole moments in the opposite direction across the entire plane, and the orientation of all dipoles in MoS_2 is from S atom layer to Mo atom layer, as shown in Fig. 5. The small angle of S-Mo-S (86.803°) makes the electronegative S atoms prevent the electronegative O atoms from coming close to Mo atoms, and MoS_2 is difficult to form a strong orientation force with HCHO. Therefore, the adsorption strength of HCHO on graphene and MoS_2 is weak. Unlike graphene, InP_3 monolayer has polar bonds, which are also different from MoS_2 because its electropositive atoms (In) are not protected by electronegative atoms (P). Strong dipole-dipole force can be formed between the dipole moment existed in InP_3 and HCHO, which may greatly enhance their interaction. Compared with

MoS_2, the structure of InP_3 monolayer is close to a plane, which makes it easier for HCHO to adsorb onto its favourite position, that is, O atom on the top of electropositive atom and C atom on the top of electronegative atom. The enhanced dipole-dipole force results in a higher E_a value.

The above analyses show that the interaction between HCHO and these 2D materials may be adjusted by applying strain to the material. Take MoS_2 as an example, the strain may increases the angle of S-Mo-S and thus reduce the shielding effect of S atoms to Mo atoms. Kou et al. reported the strain engineering of chemical adsorption on MoS_2 monolayer [40]. It was found that the charge transfer in the strain-free layer is limited between the gas molecule and the most adjacent S atom, and by contrast some electrons transfer to Mo atoms and become slightly delocalized after applying strain on the monolayer. As a result, the gas molecules are getting closer to the MoS_2 monolayer, which increases the absolute value of E_a.

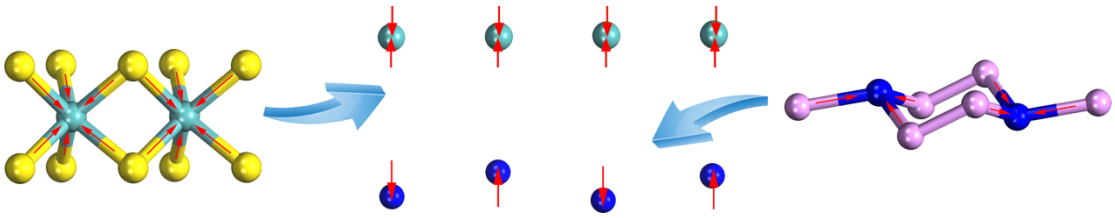

Fig. 5 The partial structures of MoS_2 (left) and InP_3 (right) and the red arrow present the orientations of the dipole of chemical bonds, between them are the metal atoms extracted from each structure and present the orientations of the dipole moment.

3.3 Enhancement of HCHO sensing performance by strain engineering

To confirm that the adsorption strength can be tuned by the application of strain on monolayer, the adsorption of HCHO onto the strained InP_3 monolayer was calculated, in which four typical strained states (2%, 4%, 6% and 8%)

along *a*-direction were implemented. The structure of InP_3 monolayer affected by strain can be seen in Fig. S2.

Fig. 6 shows the changes in a few parameters caused by strain, including the distance between In2 atom and O atom ($d_{In2\text{-}O}$), adsorption energy and the rate of change of distance between In1 atom and P1 atom (R_d). The R_d is defined as:

$$R_d = \left| d'_{In1\text{-}P1} - d_{In1\text{-}P1} \right| / (d_{In1\text{-}P1}) \quad (3)$$

where $d_{In1\text{-}P1}$ and $d'_{In1\text{-}P1}$ are the distance between In1 atom and P1 atom of InP_3 monolayer before and after adsorption of HCHO, respectively.

As shown in Fig. 6, E_a (blue line) of HCHO/strained-InP_3 system briefly increase as the strain rises from 0 to 2%, then decrease with the rising strain from 2% to 8%. After applying the strained state of 4% to InP_3 monolayer, the absolute value of E_a is larger than pristine InP_3, and this value progressively increase as the strain rises. It also shows charge transfer (the upper right corner of Fig. 6) systematically enhanced with increasing strain, going from -0.368 e at 0% strain to -0.408 e at 4% strain according to Mulliken charge analysis. It is clear that adsorption strength of HCHO on InP_3 can be enhanced by the application of strain, thus the performance of HCHO sensor based on strained InP_3 can also be promoted.

In Fig. 6, the variation of R_d (red line) with strain is almost the same as E_a, except that the value of R_d is always greater than that of the pristine InP_3. A continuous reduction of the value of $d_{In2\text{-}O}$ (black line) is caused by decrease of the shielding effect of P1 atom on In2 atom with increasing strain. Therefore, it

is easier for O atom to get closer to In2 and form a stronger interaction. The smaller the distance is, the stronger the interaction between these two atoms is. It suggests that increasing interactions will lead to a more negative E_a value, which is why E_a will decline as the strain increases from 2% to 8%.

The following explains why 2% strain is the turning point of adsorption energy. As mentioned earlier, the E_a of HCHO/InP_3 system is related to the distance of In1-P1. This is because the most favourable adsorption positions of the HCHO molecule adsorbed on InP_3 monolayer are O atom onto In1 atom and C atom onto P1 atom, respectively. As shown in Fig. S2, it was found that the adsorption process has caused obvious geometric changes on the monolayer. After InP_3 monolayer was strained, the In1-P1 distance increased, which means that the R2 ring needs more energy to distort itself to satisfy the adsorption of HCHO molecule on its favourable position. As a result, the adsorption strength decreases, in other words, the value of E_a increases. Therefore, E_a of HCHO adsorption increases first and then decreases with increasing strain.

When it comes to C_2H_5OH, the variation of E_a completely differs from HCHO, as shown in Table. S1. The absolute value of E_a is 1.1186 eV when C_2H_5OH adsorbed on pristine InP_3 monolayer. It decreases from 1.0589 eV to 0.9791 eV as the strain increases from 2% to 8%. The charge transfer also decrease with increasing strain, which is opposite of HCHO. Therefore, to a certain extent, strain can improve the selectivity of HCHO sensor based on InP_3 monolayer.

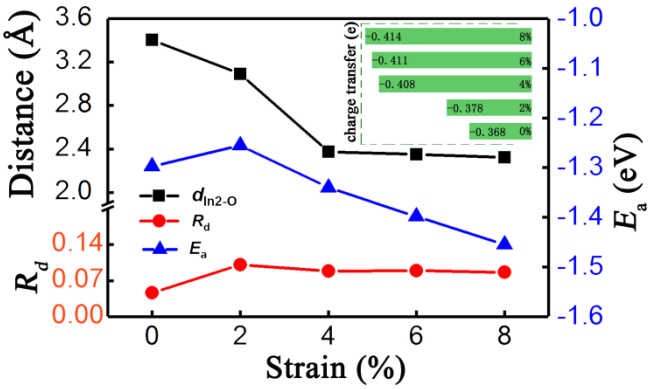

Fig. 6 The change curves of E_a (blue), R_d (red) and d_{In2-O} (black) accompany with strain in HCHO/strained-InP_3 systems. The insert presents the charge transfer of the HCHO/strained-InP_3 systems.

The DOS, PDOS and the band structure of HCHO onto 8%-strained InP_3 were also calculated and described in Fig. 7. As shown in the Fig. 7(a), the new peak appearing near the Fermi level (localized at -0.0797 eV) in DOS and the strong hybridization of orbitals in the PDOS reveal that the strong interaction between HCHO molecule and 8%-strained InP_3, which is consistent with previous result that the strain can increase adsorption strength between HCHO and InP_3. As for the band structure, when HCHO adsorbed onto the 8%-strained InP_3, band gap [see Fig. 7(b)] decreased from 0.741 eV to 0.509 eV, indicating the conductivity has a significant increase compared with that of pristine InP_3, which can be explained by the appearance of the new peak near the Fermi level in Fig 7(a).

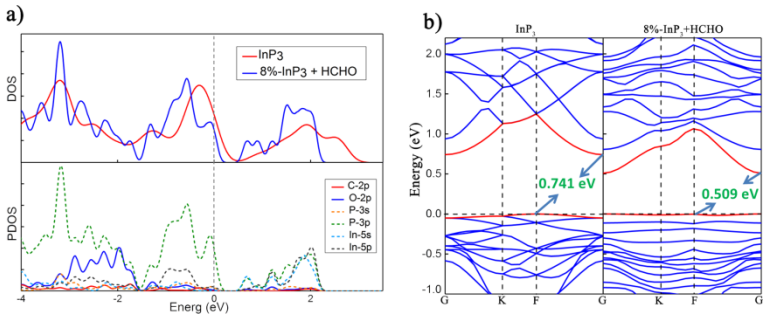

Fig. 7. (a). The total (up) and partial (down) densities of states. (b) Band structure for HCHO adsorbed on 8%-strained InP_3 monolayer based on the most stable configuration

3.4 recovery time

Since InP_3 is a potential sensitive material, it is worthy to talking about the recovery time which is one of the important factors for gas sensor. According to the transition state theory [41], the recovery time τ can be calculated by the formula (4):

$$\tau = \omega^{-1} \exp(E^*/K_B T) \qquad (4)$$

where T is the temperature, K_B is the Boltzmann' Constant, E^* is the desorption energy barrier and ω is the attempt frequency. The transition state of desorption process of HCHO from pristine InP_3 and 8% strained InP_3 can be found by calculating the minimum-energy path (MEP) [42] and then calculated the value of E^*. The initial state was the configuration with the HCHO adsorbed on InP_3, and the final state was set to be the configuration that HCHO parallel with the InP_3 at a distance of 3Å above the favourite adsorption sites. As a result, the calculated desorption energy barrier for both of these two systems are equal to their adsorption energy, which are 1.2974 eV and 1.4547 eV, respectively. The higher desorption barrier suggests a longer recovery time of HCHO on substrate at the same temperature. Suppose ω is 10^{13} s^{-1} [43, 44], then pristine InP_3 will has a recovery time of about 1 s at the temperature of 500 K and 1700 s at 400 K, and the recovery time for strained-InP_3 is 45 s at the temperature of 500 K. The results are similar with several recently reported HCHO sensors [45-47].

4 Conclusion

In conclusion, the adsorption of a few organic gases including C_2H_6, C_2H_4, C_2H_2, C_6H_6, C_2H_5OH and HCHO on InP_3 monolayer are calculated, and the properties of the gas/InP_3 systems including adsorption energy (E_a), adsorption distance (d), charge transfer (ΔQ), DOS, band structure and recovery time are obtained. With E_a of -1.2974 eV and ΔQ of -0.368 e, InP_3 monolayer has high sensitivity and selectivity to HCHO. The most favourable adsorption geometry configuration for HCHO adsorbed on InP_3 monolayer, graphene and MoS_2 were also compared, and the results prove that the E_a of HCHO absorbed on InP_3 monolayer is much larger than that of graphene and MoS_2. The phenomenon is explained by the polarity and structural feature of these 2D materials. And to further explain the importance of the material structure, the effects of strain on the HCHO/InP_3 and C_2H_5OH/InP_3 adsorption systems were also calculated. As the strain increases from 0% to 8%, the absolute value of E_a increases from 1.2974 eV to 1.4547 eV, and the charge transfer vary from -0.368 e to -0.414 e, indicating an enhancement of the interaction between HCHO and InP_3 monolayer. While for C_2H_5OH, adsorption strength and charge transfer both decreases. These results show that strained InP_3 monolayer is more sensitive and selective to HCHO than the pristine. The theoretical calculations suggest that InP_3 monolayer could be an extremely promising sensor material for the detection of HCHO. More importantly, application of strain on the sensitive material is proven to be an efficient way to improve the performance of HCHO sensor, which may shed a light on the related research.

Acknowledgements

This work is co-supported by the National Natural Science Foundation of China under Grant 51706029, Guangdong Science and Technology Program (No.2017A050506053, No.2017A010106005) and the Fundamental Research Funds for the Central Universities under Grant 2018CDXYGD0017.

References

[1] T.I.T. Akamatsu, A. Tsuruta, W. Shin, Selective Detection of Target Volatile Organic Compounds in Contaminated Humid Air Using a Sensor Array with Principal Component Analysis, Sensors (Basel, Switzerland), 17 (2017).

[2] L. Zhu, W. Zeng, H. Ye, Y. Li, Volatile organic compound sensing based on coral rock-like ZnO, Materials Research Bulletin, 100 (2018) 259-264.

[3] J. Zhang, Z. Qin, D. Zeng, C. Xie, Metal-oxide-semiconductor based gas sensors: screening, preparation, and integration, Physical Chemistry Chemical Physics, 19 (2017) 6313-6329.

[4] O. Lupan, V. Postica, V. Cretu, N. Wolff, V. Duppel, L. Kienle, R. Adelung, Single and networked CuO nanowires for highly sensitive p-type semiconductor gas sensor applications, Physica Status Solidi-Rapid Research Letters, 10 (2016) 260-266.

[5] Y. Li, N. Chen, D. Deng, X. Xing, X. Xiao, Y. Wang, Formaldehyde detection: SnO_2 microspheres for formaldehyde gas sensor with high sensitivity,

fast response/recovery and good selectivity, Sensors and Actuators B-Chemical, 238 (2017) 264-273.

[6] L. Meng, Q. Xu, Z. Sun, G. Li, S. Bai, Z. Wang, Y. Qin, Enhancing the performance of room temperature ZnO microwire gas sensor through a combined technology of surface etching and UV illumination, Materials Letters, 212 (2018) 296-298.

[7] C. Li, J. Huang, H. Zhu, L. Liu, Y. Feng, G. Hu, X. Yu, Dual-emitting fluorescence of Eu/Zr-MOF for ratiometric sensing formaldehyde, Sensors and Actuators B-Chemical, 253 (2017) 275-282.

[8] S. Ishihara, J. Labuta, T. Nakanishi, T. Tanaka, H. Kataura, Amperometric Detection of Sub-ppm Formaldehyde Using Single-Walled Carbon Nanotubes and Hydroxylamines: A Referenced Chemiresistive System, Acs Sensors, 2 (2017) 1405-1409.

[9] W. Yuan, G. Shi, Graphene-based gas sensors, Journal of Materials Chemistry A, 1 (2013) 10078-10091.

[10] F. Schedin, A.K. Geim, S.V. Morozov, E.W. Hill, P. Blake, M.I. Katsnelson, K.S. Novoselov, Detection of individual gas molecules adsorbed on graphene, Nature Materials, 6 (2007) 652-655.

[11] O. Leenaerts, B. Partoens, F.M. Peeters, Adsorption of H_2O, NH_3, CO, NO_2, and NO on graphene: A first-principles study, Physical Review B, 77 (2008).

[12] X. Chen, L. Xu, L.-L. Liu, L.-S. Zhao, C.-P. Chen, Y. Zhang, X.-C. Wang, Adsorption of formaldehyde molecule on the pristine and transition metal doped graphene: First-principles study, Applied Surface Science, 396 (2017) 1020-1025.

[13] T. Zhang, H. Sun, F. Wang, W. Zhang, J. Ma, S. Tang, H. Gong, J. Zhang, Reversible adsorption/desorption of the formaldehyde molecule on transition metal doped graphene by controlling the external electric field: first-principles study, Theoretical Chemistry Accounts, 136 (2017).

[14] Q. Zhou, L. Yuan, X. Yang, Z. Fu, Y. Tang, C. Wang, H. Zhang, DFT study of formaldehyde adsorption on vacancy defected graphene doped with B, N, and S, Chemical Physics, 440 (2014) 80-86.

[15] J. Prasongkit, R.G. Amorim, S. Chakraborty, R. Ahuja, R.H. Scheicher, V. Amornkitbamrung, Highly Sensitive and Selective Gas Detection Based on Silicene, Journal of Physical Chemistry C, 119 (2015) 16934-16940.

[16] M.M. Monshi, S.M. Aghaei, I. Calizo, Doping and defect-induced germanene: A superior media for sensing H_2S, SO_2, and CO_2 gas molecules, Surface Science, 665 (2017) 96-102.

[17] N. Liu, S. Zhou, Gas adsorption on monolayer blue phosphorus: implications for environmental stability and gas sensors, Nanotechnology, 28 (2017).

[18] V. Nagarajan, R. Chandiramouli, Adsorption of NO_2 molecules on armchair phosphorene nanosheet for nano sensor applications - A

first-principles study, Journal of Molecular Graphics & Modelling, 75 (2017) 365-374.

[19] C. Tan, Z. Lai, H. Zhang, Ultrathin Two-Dimensional Multinary Layered Metal Chalcogenide Nanomaterials, Advanced Materials, 29 (2017).

[20] H. Yuan, L. Kong, T. Li, Q. Zhang, A review of transition metal chalcogenide/graphene nanocomposites for energy storage and conversion, Chinese Chemical Letters, 28 (2017) 2180-2194.

[21] N. Miao, B. Xu, N.C. Bristowe, J. Zhou, Z. Sun, Tunable Magnetism and Extraordinary Sunlight Absorbance in Indium Triphosphide Monolayer, J Am Chem Soc, 139 (2017) 11125-11131.

[22] N. Kinomura, K. Terao, S. Kikkawa, H. Horiuchi, M. Koizumi, H. Setoguchi, SYNTHESIS AND CRYSTAL-STRUCTURE OF INP_3, Materials Research Bulletin, 18 (1983) 53-57.

[23] J. Liu, C.-S. Liu, X.-J. Ye, X.-H. Yan, Monolayer InP_3 as a reversible anode material for ultrafast charging lithium- and sodium-ion batteries: a theoretical study, Journal of Materials Chemistry A, 6 (2018) 3634-3641.

[24] Y. Yuan, Y. Wang, M. Wang, J. Liu, C. Pei, B. Liu, H. Zhao, S. Liu, H. Yang, Effect of Unsaturated Sn Atoms on Gas-Sensing Property in Hydrogenated SnO_2 Nanocrystals and Sensing Mechanism, Scientific Reports, 7 (2017).

[25] Z. Bo, M. Yuan, S. Mao, X. Chen, J. Yan, K. Cen, Decoration of vertical graphene with tin dioxide nanoparticles for highly sensitive room temperature

formaldehyde sensing, Sensors and Actuators B-Chemical, 256 (2018) 1011-1020.

[26] S. Zhang, Z. Yan, Y. Li, Z. Chen, H. Zeng, Atomically thin arsenene and antimonene: semimetal-semiconductor and indirect-direct band-gap transitions, Angew Chem Int Ed Engl, 54 (2015) 3112-3115.

[27] A. Abbasi, J.J. Sardroodi, A highly sensitive chemical gas detecting device based on N-doped ZnO as a modified nanostructure media: A DFT plus NBO analysis, Surface Science, 668 (2018) 150-163.

[28] Y. Fan, J. Zhang, Y. Qiu, J. Zhu, Y. Zhang, G. Hu, A DFT study of transition metal (Fe, Co, Ni, Cu, Ag, Au, Rh, Pd, Pt and Ir)-embedded monolayer MoS_2 for gas adsorption, Computational Materials Science, 138 (2017) 255-266.

[29] M.A. Bissett, M. Tsuji, H. Ago, Strain engineering the properties of graphene and other two-dimensional crystals, Phys Chem Chem Phys, 16 (2014) 11124-11138.

[30] J.P. Perdew, K. Burke, M. Ernzerhof, Generalized gradient approximation made simple, Physical Review Letters, 77 (1996) 3865-3868.

[31] R. Carbo-Dorca, P. Bultinck, Quantum mechanical basis for Mulliken population analysis, Journal of Mathematical Chemistry, 36 (2004) 231-239.

[32] S. Basu, P. Bhattacharyya, Recent developments on graphene and graphene oxide based solid state gas sensors, Sensors and Actuators B-Chemical, 173 (2012) 1-21.

[33] Q. He, S. Wu, Z. Yin, H. Zhang, Graphene-based electronic sensors, Chemical Science, 3 (2012) 1764-1772.

[34] L. Duan, Z. Bo, X. Chen, H. Qi, J. Yan, K. Cen, Ab initio characterization and experimental validation on the roles of oxygen-containing groups in graphene based formaldehyde sensors, Analyst, 143 (2017) 106-115.

[35] W. Wei, S. Guo, C. Chen, L. Sun, Y. Chen, W. Guo, S. Ruan, High sensitive and fast formaldehyde gas sensor based on Ag-doped $LaFeO_3$ nanofibers, Journal of Alloys and Compounds, 695 (2017) 1122-1127.

[36] D. Ma, W. Ju, T. Li, G. Yang, C. He, B. Ma, Y. Tang, Z. Lu, Z. Yang, Formaldehyde molecule adsorption on the doped monolayer MoS_2: A first-principles study, Applied Surface Science, 371 (2016) 180-188.

[37] J. Dai, J. Yuan, P. Giannozzi, Gas adsorption on graphene doped with B, N, Al, and S: A theoretical study, Applied Physics Letters, 95 (2009).

[38] B. Akdim, R. Pachter, S. Mou, Theoretical analysis of the combined effects of sulfur vacancies and analyte adsorption on the electronic properties of single-layer MoS_2, Nanotechnology, 27 (2016).

[39] K.F. Mak, C. Lee, J. Hone, J. Shan, T.F. Heinz, Atomically Thin MoS_2: A New Direct-Gap Semiconductor, Physical Review Letters, 105 (2010).

[40] L. Kou, A. Du, C. Chen, T. Frauenheim, Strain engineering of selective chemical adsorption on monolayer MoS_2, Nanoscale, 6 (2014) 5156-5161.

[41] Y.-H. Zhang, Y.-B. Chen, K.-G. Zhou, C.-H. Liu, J. Zeng, H.-L. Zhang, Y. Peng, Improving gas sensing properties of graphene by introducing dopants and defects: a first-principles study, Nanotechnology, 20 (2009).

[42] G. Henkelman, B.P. Uberuaga, H. Jonsson, A climbing image nudged elastic band method for finding saddle points and minimum energy paths, Journal of Chemical Physics, 113 (2000) 9901-9904.

[43] A. Kokalj, Formation and structure of inhibitive molecular film of imidazole on iron surface, Corrosion Science, 68 (2013) 195-203.

[44] S. Weigelt, C. Busse, C. Bombis, M.M. Knudsen, K.V. Gothelf, T. Strunskus, C. Woll, M. Dahlbom, B. Hammer, E. Laegsgaard, F. Besenbacher, T.R. Linderoth, Covalent interlinking of an aldehyde and an amine on a Au(111) surface in ultrahigh vacuum, Angewandte Chemie-International Edition, 46 (2007) 9227-9230.

[45] H. Yu, T. Yang, R. Zhao, B. Xiao, Z. Li, M. Zhang, Fast formaldehyde gas sensing response properties of ultrathin SnO_2 nanosheets, Rsc Advances, 5 (2015) 104574-104581.

[46] H.J. Park, N.-J. Choi, H. Kang, M.Y. Jung, J.W. Park, K.H. Park, D.-S. Lee, A ppb-level formaldehyde gas sensor based on CuO nanocubes prepared using a polyol process, Sensors and Actuators B-Chemical, 203 (2014) 282-288.

[47] R.K. Mishra, A. Kushwaha, P.P. Sahay, Influence of Cu doping on the structural, photoluminescence and formaldehyde sensing properties of SnO_2 nanoparticles, Rsc Advances, 4 (2014) 3904-3912.